Nuclear Instruments and Methods in Physics Research A 701 (2013) 186–193

Contents lists available at SciVerse ScienceDirect

Nuclear Instruments and Methods in Physics Research A

journal homepage: www.elsevier.com/locate/nima

Design of a CW high charge state heavy ion RFQ for SSC-LINAC

G. Liu [a], Y.R. Lu [a,b,*], Y. He [b,**], Z. Wang [a,**], C. Xiao [b], S.L. Gao [a], Y.Q. Yang [b], K. Zhu [a], X.Q. Yan [a], J.E. Chen [a], Y.J. Yuan [b], H.W. Zhao [b]

[a] State Key Lab of Nuclear Physics and Technology, Peking University, Beijing 100871, China
[b] Institute of Modern Physics, China Academy of Science, Lanzhou 730000, China

ARTICLE INFO

Article history:
Received 14 May 2012
Received in revised form
29 October 2012
Accepted 2 November 2012
Available online 16 November 2012

Keywords:
RFQ accelerator
High charge state
Heavy ion
Continuous wave

ABSTRACT

The new linac injector SSC-LINAC has been proposed to replace the existing Separator Sector Cyclotron (SSC). This effort is to improve the beam efficiency of the Heavy Ion Research Facility of Lanzhou (HIRFL). As a key component of the linac, a continuous-wave (CW) mode high charge state heavy ion radio-frequency quadrupole (RFQ) accelerator has been designed. It accelerates ions with the ratio of mass to charge up to 7 from 3.728 keV/u to 143 keV/u. The requirements of CW mode operation and the transportation of intense beam have been considered as the greatest challenges. The design is based on $^{238}U^{34+}$ beams, whose current is 0.5 pmA (0.5 particle mili-ampere, which is the measured 17 emA electric current divided by charge state of heavy ions). It achieves the transmission efficiency of 94% with 2508.46 mm long vanes in simulation. To improve the transmission efficiency and quality of the beams, the phase advance has been taken into account to analyze the reasons of beam loss and emittance growth. Parametric resonance and beam mismatch have been carefully avoided by adjusting the structure parameters. The parameter-sensitivity of the design is checked by transportation simulations of various input beams. To verify the applicability of machining, the effects of different vane manufacturing methods on beam dynamics are presented in this paper.

1. Introduction

The Heavy Ion Research Facility of Lanzhou (HIRFL) was upgraded with a multi-functional Cooler Storage Ring (CSR) at the end of 2007 [1]. The injector of CSR consists of two cyclotrons, which are a Sector Focusing Cyclotron (SFC) and a Separator Sector Cyclotron (SSC). For light ions, beams from the SFC with the energy of 5.62 MeV/u are injected into the CSR directly for the Super-Heavy Elements (SHE) experiment, while for heavy ions, they are transported from the SFC into the SSC first ,accelerated to 10.06 MeV/u, and then injected into the CSR. However, this scheme causes low beam efficiency, especially for heavy ions [2]. To solve this problem, a new linac called SSC-LINAC has been proposed as an injector to replace the SFC. The SSC-LINAC consists of a superconducting high charge state ECR ion source, a continuous-wave normal-conducting RFQ, a rebuncher and four IH-DTL cavities [3], see Fig. 1.

The RFQ accelerator is an important component in this linac injector. In the recent decades, several RFQs have been designed and constructed for high charge state or high intensity heavy ion beams, a few of them working in CW mode. For example, the GSI HLI-RFQ, which accelerates high charge state U^{28+} ions with the duty factor of 50% [4, 5]; the GSI HSI-RFQ accelerates the 16.5 emA beam of U^{4+} with the duty factor of not more than 30% [6, 7]; the RFQ for RILAC in RIKEN is a variable-frequency machine for heavy ion beams [8]; the ISAC RFQ of TRIUMF is a low charge state RFQ but works in CW mode [9]; another CW heavy ion RFQ is one of the two RFQs in SPIRAL 2 project [10], which is designed for 1 mA ion beams with the ratio of charge to mass $q/A=1/3$. The SSC-LINAC RFQ will work in CW mode to match the operation of SSC. The machine has to transport $^{238}U^{34+}$ beams with the current of 0.5 pmA, i.e. 17e mA. It is a very intense beam for such high charge state heavy ions. These requirements bring challenges to the beam dynamics, structure and cooling system design. Since the high charge state will enhance the space charge force, a wide safety margin should be left for different species of ions and beam intensities. Some strategies such as a special match design method have been applied to the design process.

2. Design strategy

The code PARMTEQM [11] is used to carry out the beam dynamics design. The range of some important parameters should be determined as the first step. In RFQ, the radial focusing

* Corresponding author at: State Key Lab of Nuclear Physics and Technology, Peking University, Beijing 100871, China. Tel.: +86 1062755023; fax: +86 1062751875.
** Corresponding authors.
E-mail addresses: yrlu@pku.edu.cn (Y.R. Lu), hey@impcas.ac.cn (Y. He), wangzhi@pku.edu.cn (Z. Wang).

0168-9002/$ - see front matter © 2012 Elsevier B.V. All rights reserved.
http://dx.doi.org/10.1016/j.nima.2012.11.017

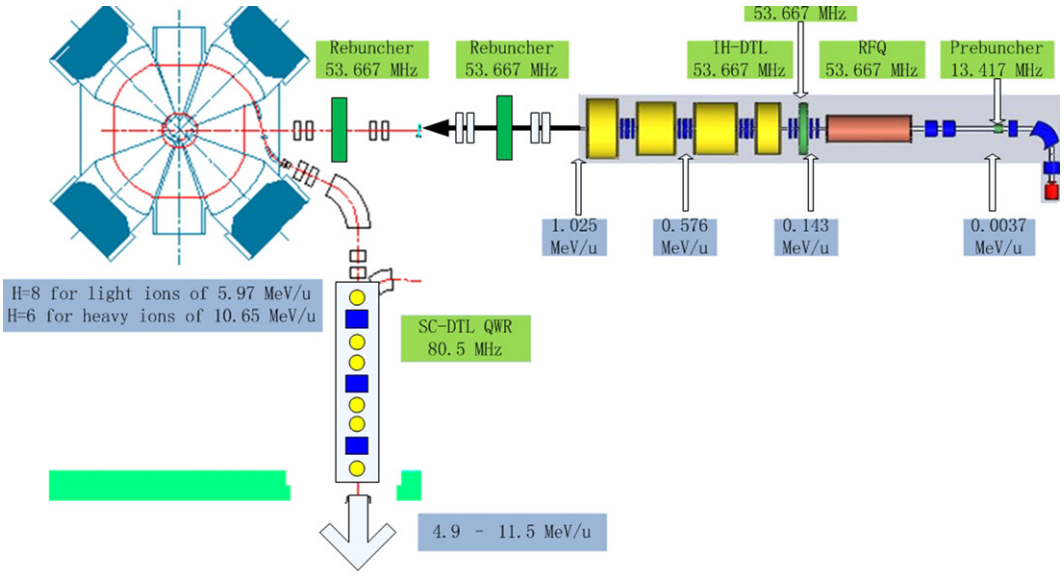

Fig. 1. Layout of the SSC-LINAC [3]. The quantity H of the Separator Section Cyclotron indicates the harmonic number.

strength B is described as $B=q\lambda^2XV/(mc^2a^2)$ [12], where q is the charge state of ions, λ is the RF wavelength at the working frequency, X is the focusing parameter, V is the inter-vane voltage, M is the relativistic mass of ions, c is the velocity of light, and a is the aperture of RFQ. Then for heavy ions, it is reasonable to obtain enough focusing strength by increasing the charge state of the ions or reducing the aperture and frequency of the RFQ. Smaller aperture causes a lower transverse acceptance, which is an obstacle to increase the beam current. Another way to improve the focusing is using higher inter-vane voltage. This is limited by the restraint of CW operation mode, as the inter-vane voltage V should be low enough to reduce the power consumption and the risk of RF sparking. Furthermore, the vane modulation factor m should be less than 2 for CW operation and intense beams.

The conventional design strategy of the PARMTEQM divides RFQ into four sections: the RM (radial matching) section, the SHAPER section, the GB (gentle buncher) section, and the ACC (accelerating) section. This method keeps a constant radial-focusing strength along the RFQ [12]. Generally, in the SHAPER section, the longitudinal accelerating field grows in order to provide the bunching force. It makes the longitudinal phase oscillation stronger, which means the phase advance of zero current σ_{0L} becomes large as well. The synchronous phase still maintains the value of nearly -90° to provide a large phase stable area. The radial-focusing strength B remains constant, which means if the longitudinal field is being increased while the transverse focusing is being reduced, then the phase advance of zero current in the transverse plane σ_{0T} will be reduced. In the following GB section, the σ_{0T} and σ_{0L} are nearly the same or even equal (the dash curves in Fig. 2(a)), which causes parametric resonance [13]. Consequently, the emittance grows obviously. If the beam current is low, this is not a critical problem; but in the high current case, such emittance growth induces serious beam loss. So the $\sigma_{0T}=\sigma_{0L}$ resonance should be avoided in the design.

Taking account of the space charge effect, the phase advance becomes [14]

$$\sigma_T^2=\sigma_{0T}^2-\Delta_{sc} \tag{1}$$

where

$$\Delta_{sc}=\frac{I\lambda^3k(1-ff)}{[r_T^3(\gamma r_L)\gamma^2]} \tag{2}$$

The subscripts T and L represent transverse and longitudinal plane, respectively; r is the RMS beam radius; γ is the relativistic parameter; I is the beam current; ff is the ellipsoid form factor; and $k=(3/8\pi)(Z_0eq/mc^2)$, where $Z_0=376.73\,\Omega$ is the free-space impedance. In RFQ, the longitudinal beam length r_L decreases in the SHAPER section due to the strengthening phase oscillation, so Δ_{sc} increases in Eq. (2), and σ_T becomes even smaller in Eq. (1), see the dash curve in Fig. 2(b). As a consequence, the beam will be mismatched [15], which will also cause the transverse emittance growth.

The design strategy should be improved to minimize the beam loss and emittance growth. From the matched beam envelope equation $\varepsilon_{Tn}=r_T^2\gamma\sigma_T/\lambda$ [16], the optimized method is to adjust the transverse phase advance σ_T to confine the variation of beam size and emittance. To keep the balance of the focusing force and defocusing effect caused by the space charge force, the σ_{0T} should be increased to avoid parametric resonance. In the PARMTEQM code, the radial focusing strength B, the vane modulation factor m, and the synchronous phase ϕ_S could be modified to keep the beam matched [14,17]. The solid lines of Fig. 2(a) and (b) represent the σ_{0T}, σ_{0L} and σ_t after optimization, respectively. It shows that the curves of σ_{0T} and σ_{0L} have been separated and the σ_T in the bunching process has been enhanced effectively. Fig. 3 compares the normalized RMS emittance of the designs before and after optimization. In Fig. 3(a), the emittance in transverse plane grows significantly in the bunching process due to the parameter resonance and mismatch mentioned above, and maintains a high level through tens of cells. It causes many particles loss transversely. At the end of the GB section, the longitudinal emittance grows largely due to phase slip. This effect could be reduced if the bunching process is very gentle; however, it will lead to a longer structure. The coupling and non-linear effect makes the transverse line decline after cell-100. Due to the non-synchronous particles lost at the entrance of the ACC section, the longitudinal emittance decreases quickly. Fig. 3(b) shows the result after optimization. The emittance growth has been improved notably. A slight mismatch happened near the end of the GB section, but it caused just a small fraction of the particles loss. The number of particles lost longitudinally is also decreased. Fig. 4 demonstrates these improvements furthermore. In the traditional design before optimization, a beam loss peak locates at cell-50 of the blue points, which corresponds to the emittance growth in Fig. 3(a). After the peak, there still exists a platform on the blue points, which means many

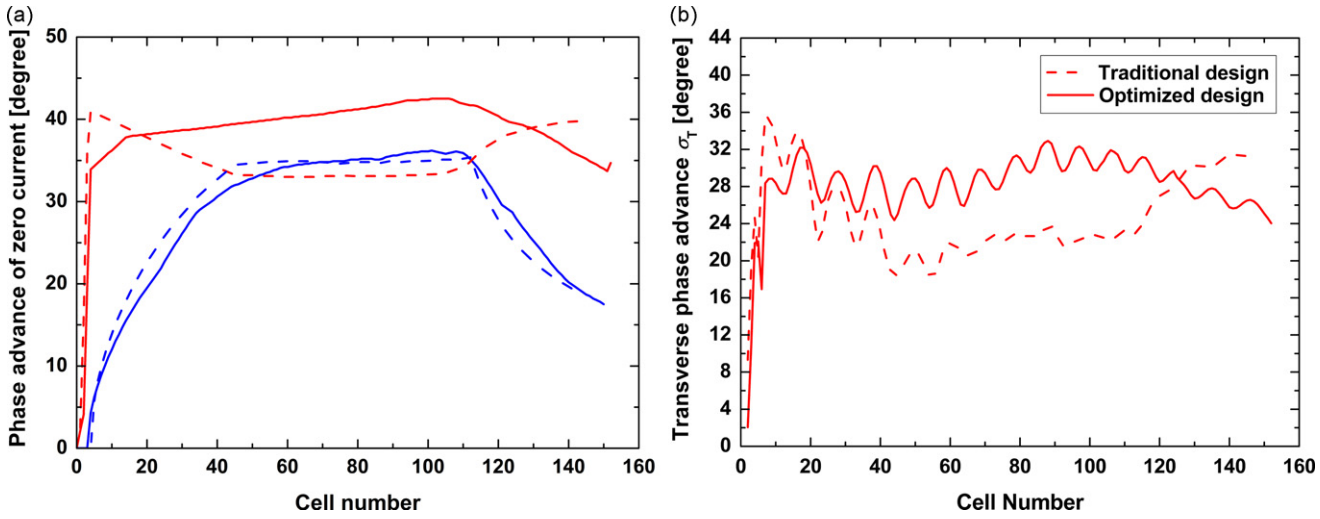

Fig. 2. Comparison of the phase advance between the traditional and optimized design. (a) Phase advance of zero current in the transverse (red) and longitudinal (blue) planes for both the traditional design (dash line) and optimized one (solid line) and (b) phase advance with current in the transverse plane for both designs. Cell- 0 is the entrance of the RFQ in all the figures, including these two. (For interpretation of the references to colour in this figure legend, the reader is referred to the web version of this article.)

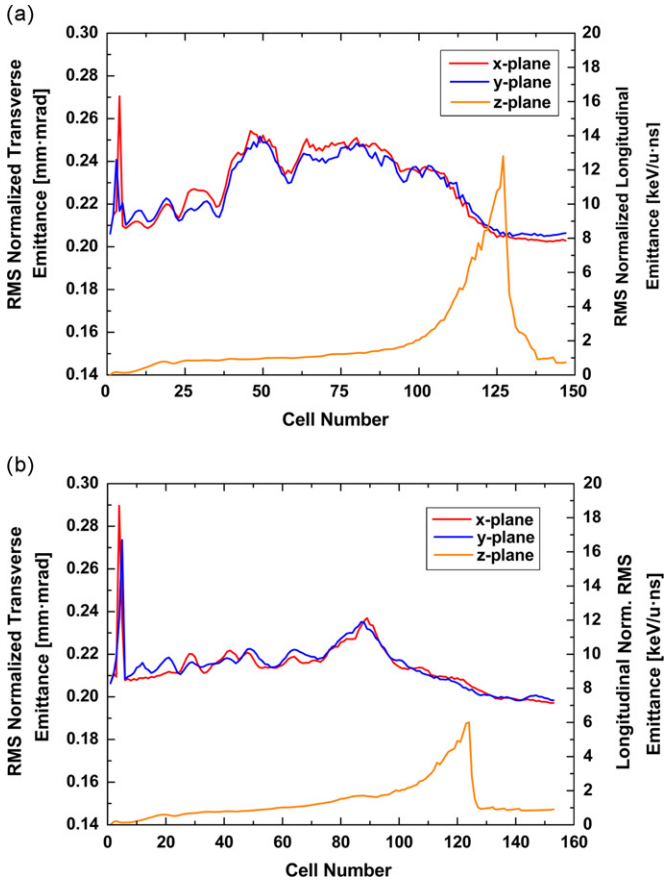

Fig. 3. Comparison of the normalized RMS emittance between the traditional and optimized design: (a) traditional design and (b) optimized design.

particles are lost from cell 60 to 100. This also corresponds to the large emittance area in Fig. 3(a). In cells 110–120, there is another peak, which is caused by longitudinal phase slip and non-linear effect. It also corresponds to the emittance curves in Fig. 3(a). Also in Fig. 4, the sum of lost particles in the optimized design reduces obviously. The first peak of the red points relates to the transverse emittance growth in Fig. 3(b), where losses have been

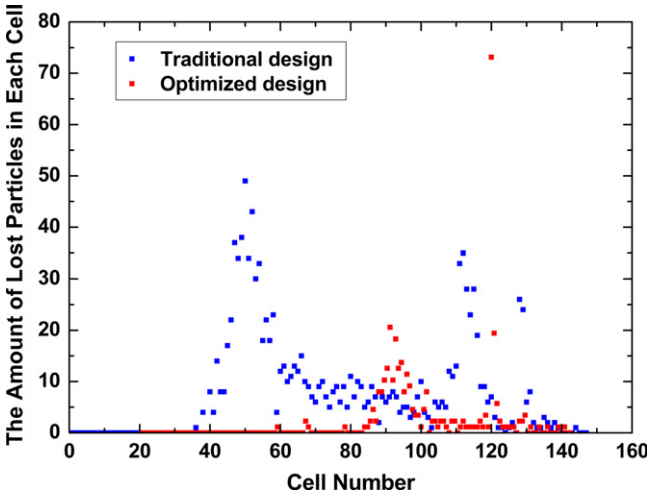

Fig. 4. Comparison of beam loss between the traditional and optimized design. (For interpretation of the references to colour in this figure legend, the reader is referred to the web version of this article.)

largely decreased. The second peak at around cell-120 relates to the longitudinal plane. Though the beam loss in this direction happens mainly in two cells, which are actually the bottle neck between bunching and acceleration sections, the sum of lost particles has been cut. Fig. 5 presents the RMS beam size in the optimized design. The transverse beam size has just a small oscillation around a constant because of the improvement in emittance growth and phase advance. The blue line declines in the SHAPER section for the reason of strengthening phase oscillation longitudinally, and it also remains nearly constant during the bunching process. Later, it rises as the emittance grows and drops due to phase slip. In the ACC section, the longitudinal beam size grows because of the acceleration.

3. Results of simulation

The main parameters of SSC-LINAC RFQ are listed in Table 1. The frequency of SSC-LINAC RFQ is chosen as 4 times that of SSC which is on 13.417 MHz [3]. The minimum transverse acceptance

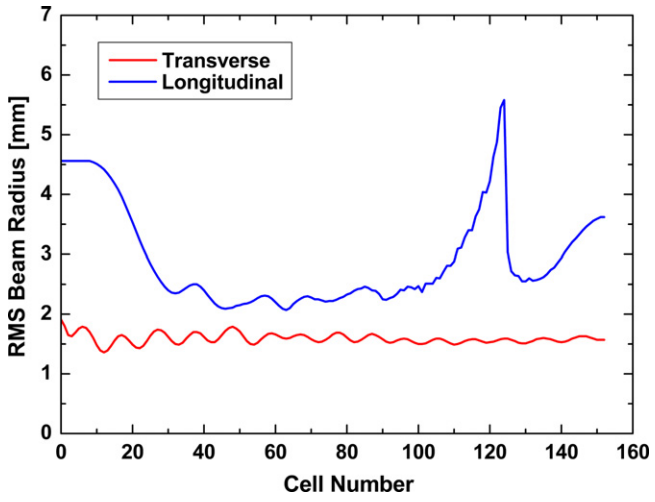

Fig. 5. RMS beam radius versus cell number in the optimized design. (For interpretation of the references to colour in this figure legend, the reader is referred to the web version of this article.)

Table 1
Parameters of beam dynamics design.

Parameters	Values
Frequency (MHz)	53.667
Ions	$^{238}U^{34+}$
Ratio of charge to mass	1/7
Beam current (pmA)	0.5
Input energy (keV/u)	3.728
Output energy (keV/u)	143
Duty factor	100%
Inter-vane voltage (kV)	70
Maximum surface field (MV/m)	14.0928
Kilpatrick coefficient	1.523
Minimum Aperture a cm	0.472
Maximum modulation Factor m	1.94
Synchronous Phase ϕ_S	$-90°$to$-30°$
Minimum transverse acceptance (mm · mrad)	0.938
Input transverse emit. (Norm. RMS) (mm · mrad)	0.206
Output transverse emit. (Norm. RMS) (mm · mrad)	0.201
Output longitudinal emit. (Norm. RMS) (keV/u ns)	0.9112
Length of the vanes (cm)	250.846
Cell number	153
Transmission efficiency (0.5 pmA $^{238}U^{34+}$ beams)	94.1%
Transmission efficiency (17e mA $^{7}Li^{1+}$ beams)	94.3%

is calculated by the following equation [18]:

$$Acc = \frac{a^2\sigma_{T0}}{2\lambda}\sqrt{\left(1-\frac{B}{4\pi^2}\right)^3 \Big/ \left(1+\frac{B}{4\pi^2}\right)} \quad (3)$$

The number of particles in the simulation is 5000, and the energy limit for the longitudinal energy difference is 10.2 MeV. For 0.5 pmA $^{238}U^{34+}$ beams, the transmission efficiency reaches 94%; and for 17 emA $^{7}Li^{1+}$ beams, the efficiency could be a little higher. Fig. 6 shows the transverse beam envelope and the longitudinal phase space evolution along the RFQ. Beam loss occurs mainly at the GB section (around cell-93) and the entrance of the ACC section (around cell-120), which is analyzed in the previous section. Figs. 7 and 8 are the plots in phase space. The FWHM energy spread at the exit of the RFQ is approximately 3%.

4. Error analysis

In real operations, the beam quality at the entrance of the RFQ has a significant influence on the transportation. For this reason, the non-ideal input $^{238}U^{34+}$ beams have been simulated to check the sensitivity of this RFQ. The design value of beam parameters at the entrance are $\alpha=0.9$, $\beta=5.0$ cm/rad, $\varepsilon_t=0.2$ mm · mrad (Norm. RMS) and the beam current of 0.5 pmA, the energy of 3.728 keV/u with zero energy spread and 360° phase width. One parameter is changed and others are kept constant during the simulations. Fig. 9(a) is the contour map of the transmission efficiency for different input Twiss parameters. The black point in it represents the design value. The efficiency is more sensitive to α than β because for different α, especially the larger one, the beam spot changes quickly during transportation. Then it is more difficult to match the beam since the space charge force varies quickly as well. In Fig. 9(b), the current changes from 0 to 1.0 pmA and the efficiency remains relatively high under 0.6 pmA. In the beam commissioning and operation later, the beam current will start from a low level such as the order of μA, so this design leaves a margin on current for future requirement. Fig. 9(c) presents the transmission efficiency as a function of input beam energy spread. The transmission slowly declines when the input spread is less than 10%. Fig. 9(d) shows that for the design Twiss parameters used in the simulations, a large emittance (which means a large beam size and/or divergence) induces a transmission decay. Lower emittance causes transmission efficiency decreases as well because it indicates the smaller beam size and/or divergence, which enhances the space charge effect.

5. Considerations for vane manufacturing

To verify the effect of the vane manufacturing craft on the beam dynamics, the beam transportations through the vanes with different tip radii have been simulated. The vanes are usually machined by a numerical control miller. However, the tools that mill the vane tip are not the same in different crafts. One type is the ball-end milling tool [19], which cuts along a three dimension path on the vane tip as shown in Fig. 10(a). The other type is the shaped arc milling tool, of which the cutting edge is an arc as shown in Fig. 10(b). The radius of the arc equates to the radius of the vane tip [20]. The shaped tool moves along a curve in the longitudinal direction. Usually, the vane tip radius *Rho* is set to [11]

$$Rho = cr_0 \quad (4)$$

where c is a constant in the range of 0.75–1, and r_0 is the average aperture of each cell in RFQ.

If the radial focusing strength B is constant along the RFQ, the *Rho* is a constant (for constant inter-vane voltage design) since $B \propto r_0^{-2}$. Then the two milling methods above are identical in this case. To simplify the process of manufacturing, the shaped arc milling tool is better. However, if B varies along the longitudinal direction, r_0 varies as well (which is the case for this RFQ). This means that the *Rho* changes along the RFQ if c remains constant. In this case, the two types of tools will produce different vane shapes. For ball-end tools, it makes the vane with different *Rho* longitudinal. But for the shaped arc tools, since the radius of the arc is fixed, the r_0 in Eq. (4) has to be modified as follows to derive a constant vane tip radius *Rho*:

$$Rho = c\frac{\sum_i r_{0i}L_{cell,i}}{L_{total}} \quad (5)$$

in which r_{0i} is the average aperture of each cell, $L_{cell,i}$ and L_{total} are the lengths of each cell and the electrode respectively, and c is still a constant in the range of 0.75–1. If all cells have the same r_0, Eq. (5) reduces to Eq. (4). To check the difference between the constant ratio $c = Rho/r_0$ and the constant *Rho*, beam transportations in these two structures have been simulated by the PARMTEQM.

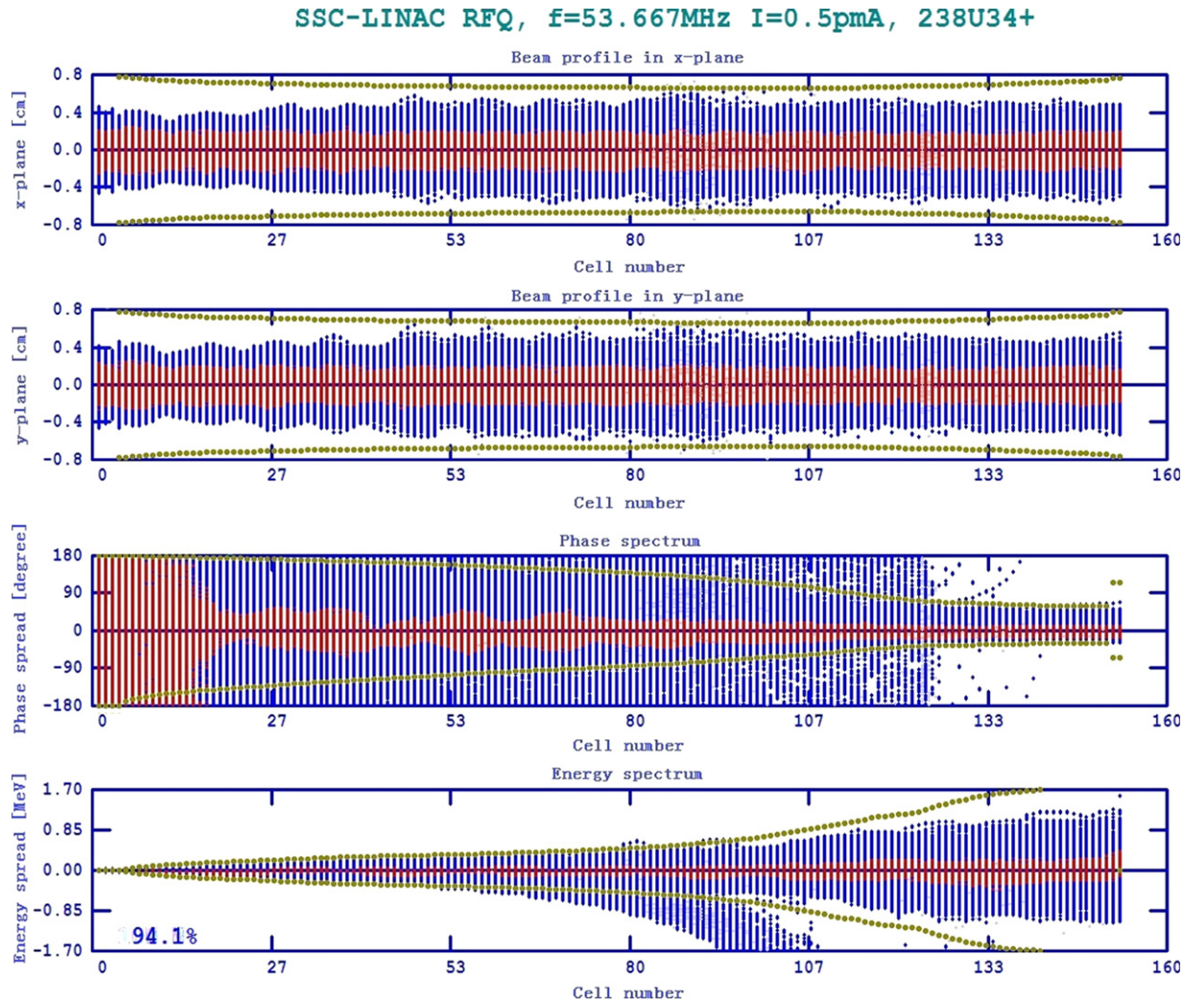

Fig. 6. Beam transmission along the RFQ. Plots from top to bottom are the beam profiles in x and y planes, phase and energy spectrums respectively.

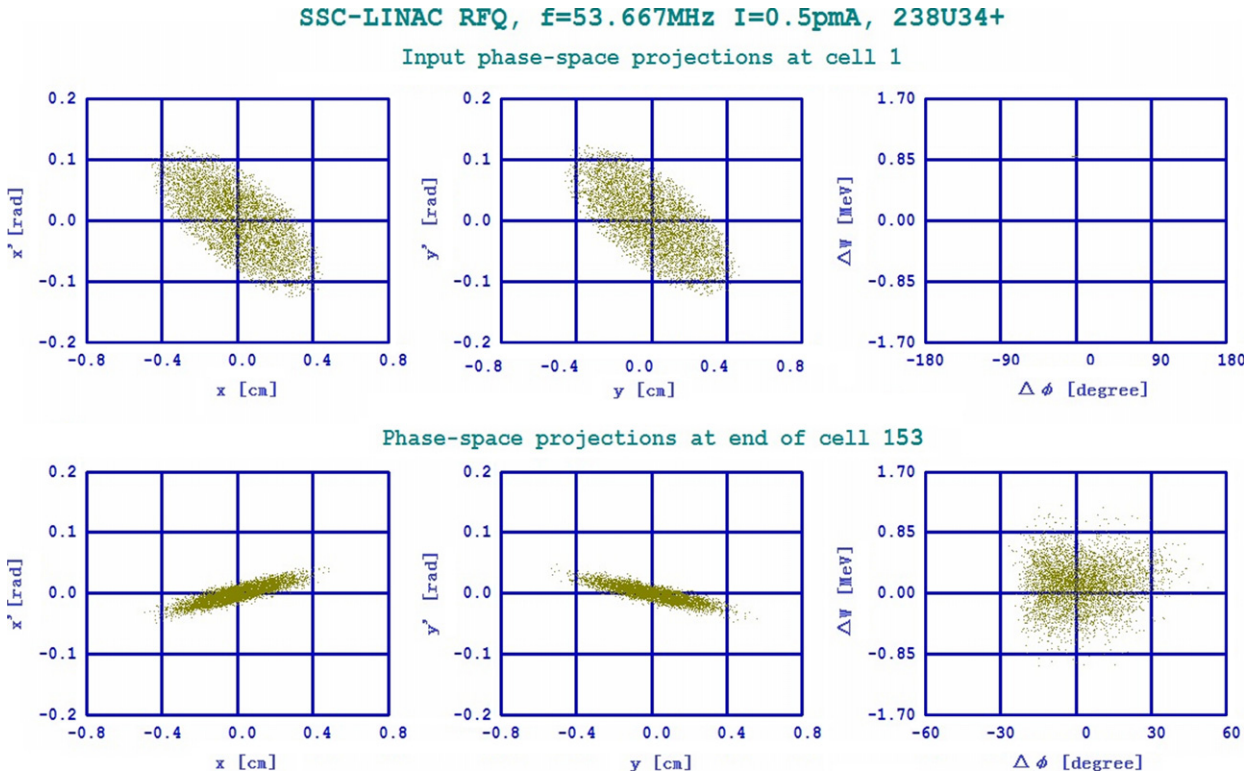

Fig. 7. Transverse phase space projection at the entrance and exit of the RFQ. The upper three figures refer to the entrance while the lower three refer to the exit. For the input beam Zero energy spread and 360° phase width are assumed, so the points in the top right box locate just on the line $dW=0.00$.

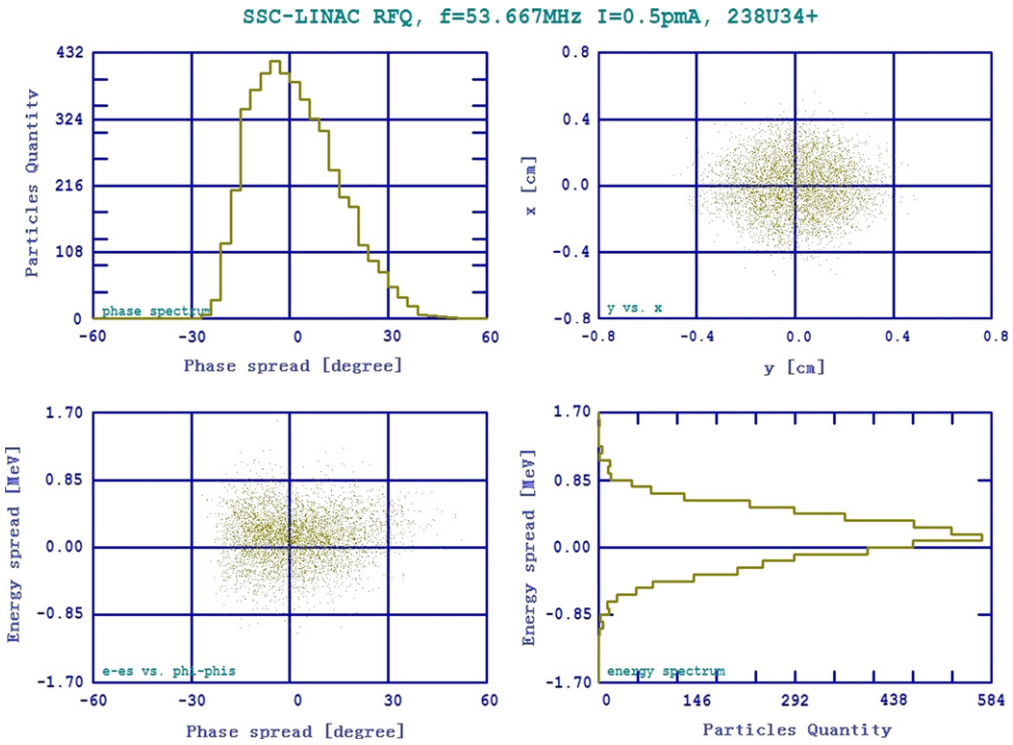

Fig. 8. Longitudinal phase space projection at the exit of the RFQ. The upper left figure shows the phase width of the beams; the upper right figure shows the particles distribution in the real space; the down left shows the particles distribution in the longitudinal phase space, and the down right presents the energy spread.

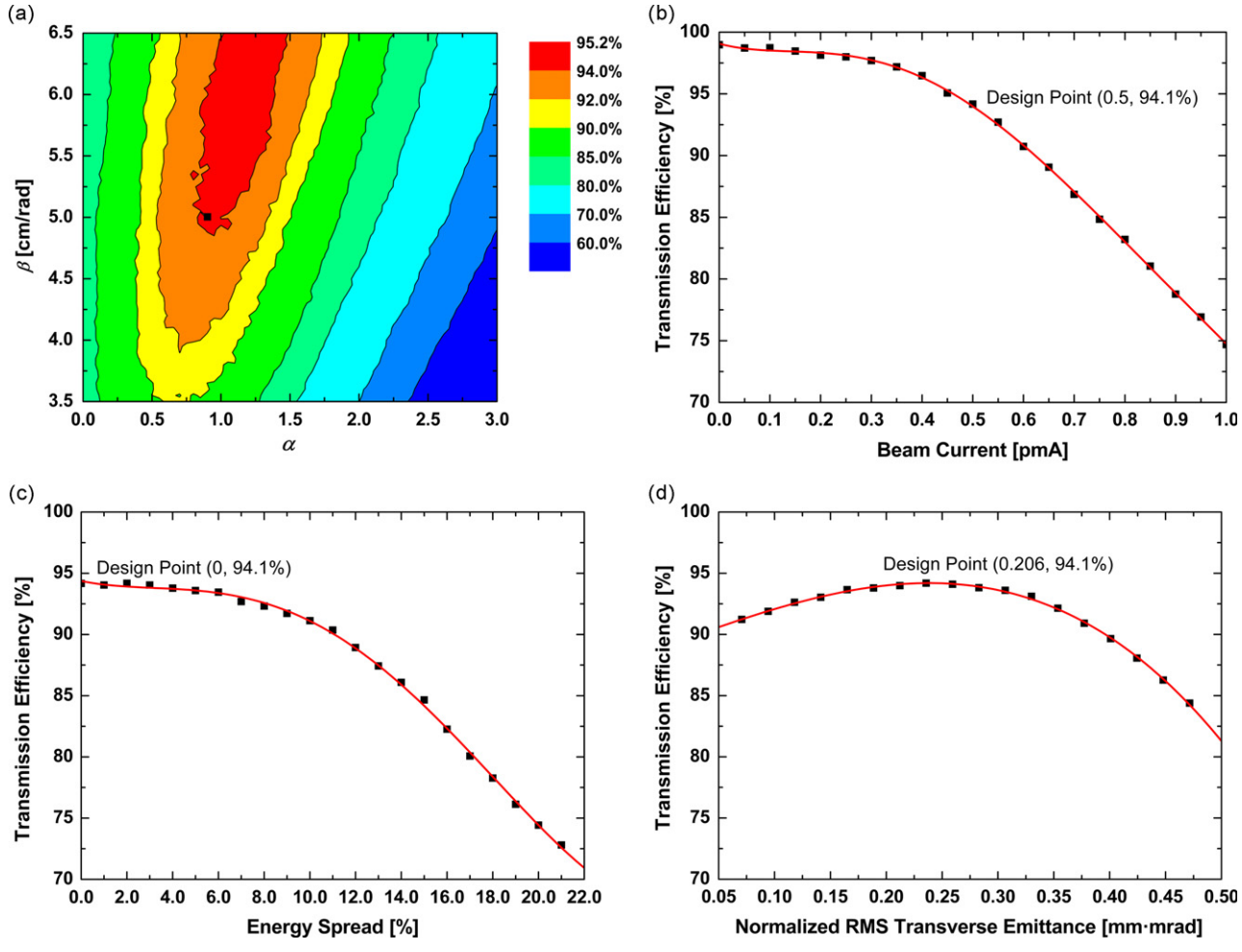

Fig. 9. Transmission efficiency of the RFQ behavior versus (a) beam Twiss parameters; (b) beam current; (c) beam energy spread and (d) beam emittance.

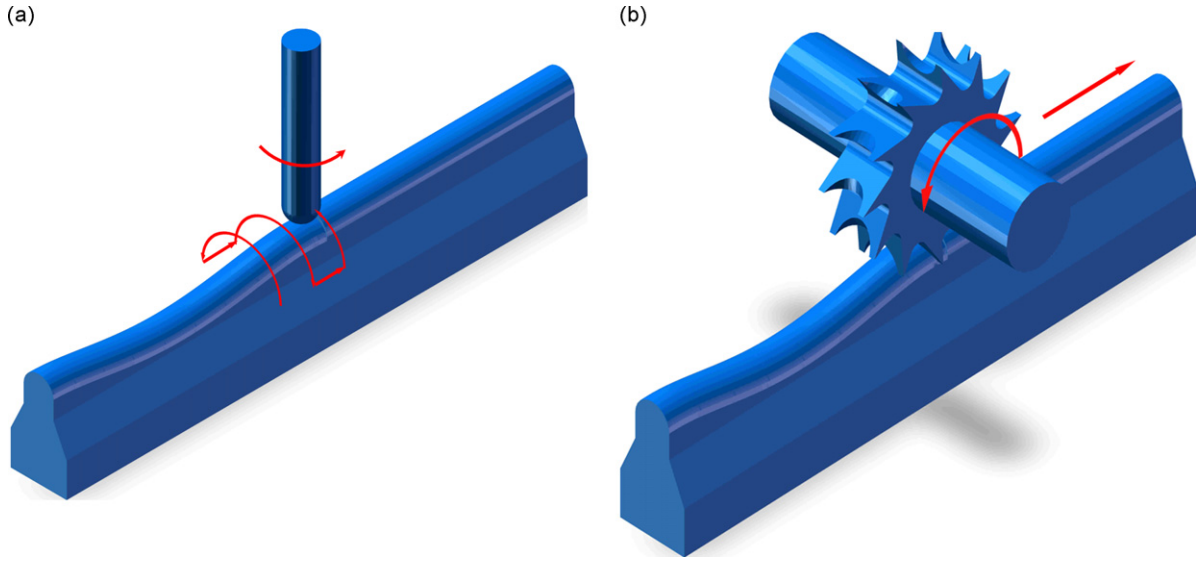

Fig. 10. Two kinds of mill tool: (a) The ball-end tool and (b) the shaped arc tool. The red curves indicate the paths of tools movement and rotation. (For interpretation of the references to colour in this figure legend, the reader is referred to the web version of this article.)

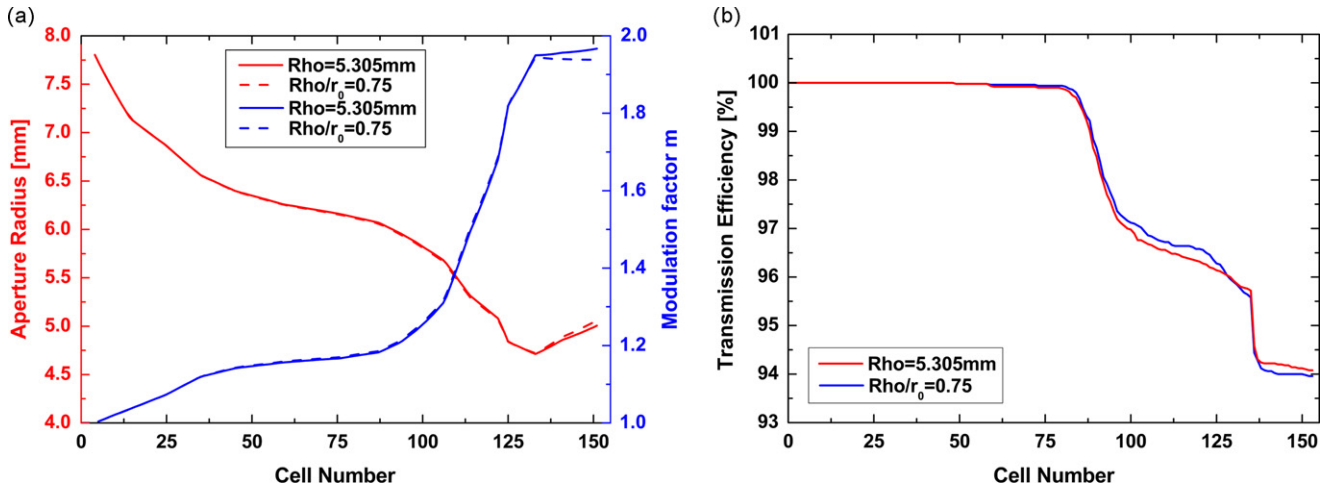

Fig. 11. Aperture radius, modulation factor and transmission efficiency of these two structure.

In the calculations, both designs have the same input file. The constant ratio Rho/r_0 is 0.75, while the constant vane tip radius is $Rho=5.305$ mm, which is derived from Eq. (5) with the average aperture of each cell. The two structures generated by the code have just a little difference on the aperture radius a and the vane modulation factor m in the ACC section, as shown in Fig. 11(a). Their transmission efficiencies are nearly the same as shown in Fig. 11(b). The potential of electric field generated by the electrodes around the beam axis could be expressed by the following equation [11]:

$$\Phi(r,\theta,z)\approx\frac{V}{2}\left\{A_0\left(\frac{r}{r_0}\right)^2\cos(2\theta)+A_1\left(\frac{r}{r_0}\right)^6\cos(6\theta)\right.$$
$$+A_{10}I_0(kr)\sin(kz)+A_{12}I_4(kr)\cos(4\theta)\sin(kz)$$
$$+A_{21}I_2(2kr)\cos(2\theta)\sin(2kz)+A_{23}I_6(2kr)\cos(6\theta)\sin(2kz)$$
$$\left.+A_{30}I_0(3kr)\sin(3kz)+A_{32}I_4(3kr)\cos(4\theta)\sin(3kz)\right\} \quad (6)$$

The difference of vane tip induces the effect on the electric field. To compare the two structures, the coefficients of the right eight terms of the potential have been calculated as shown in Fig. 12. Because these coefficients in the two cases are in the order of 10^{-2} or even lower, the difference could not affect the potential evidently. This means that the electric fields generated by these two types of electrodes have little difference. To reduce the complexity in manufacture, the vanes of the SSC-LINAC RFQ will be machined by the shaped arc milling tool, though the radial focusing strength B of the structure is variable.

6. Conclusion

To improve the beam efficiency of the HIRFL, a new linac injector SSC-LINAC is under construction. The beam dynamics design of the CW RFQ based on $^{238}U^{34+}$ ions with the beam intensity of 0.5 pmA has been studied thoroughly. The beam loss in traditional design strategy is mainly due to parametric resonance and beam mismatch, which is caused by the unsuitable phase advance of zero current per period. After the optimization of the phase advance along the RFQ, the transmission efficiency reaches 94%, and the length of the vanes is 2508.46 mm. The transportation of the intense beam for different parameters, such as the beam current, energy spread and emittance have been carried out. The results show that this design has a wide compatible margin for non-ideal input beams. Furthermore, the effects on the beam dynamics for different vane tip radii have

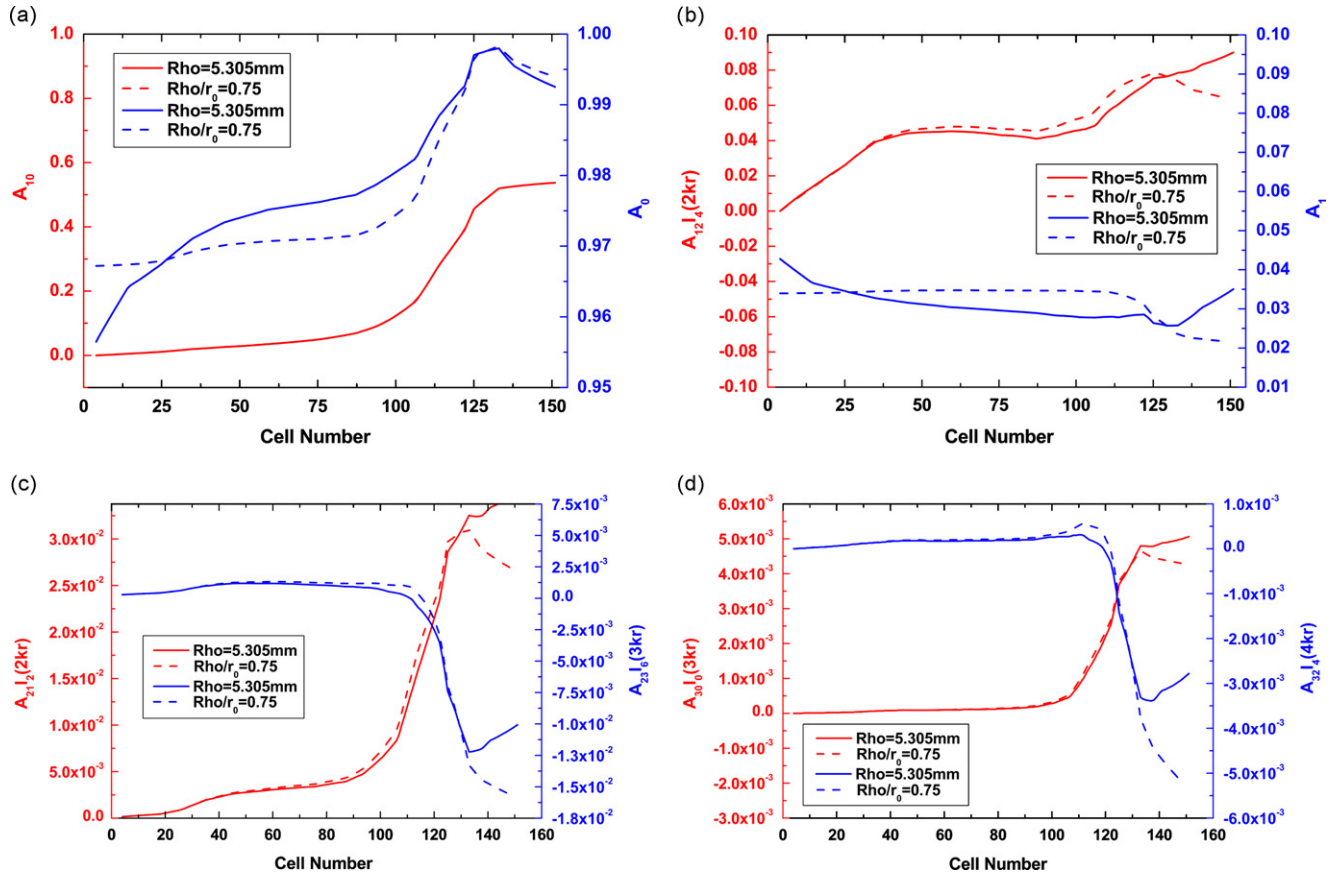

Fig. 12. Coefficients of the right eight terms of potential in the two structures. (a) A_{10}, A_0; (b) $A_{12}I_4(2kr)$ A_1; (c) $A_{21}I_2(2kr)$, $A_{23}I_6(3kr)$ and (d) $A_{30}I_0(3kr)$, $A_{32}I_4(4kr)$.

been simulated as well. The coefficients of the potential expression for these two different vane tips have a little difference. The cold model test and the high power experiment of this RFQ will be carried out in mid-2012.

Acknowledgment

The work was supported by NSFC (11079001, 10905003) and also the Linear Accelerator Center of PKU-IMPCAS. The authors want to give special thanks to Dr. Yuancun Nie and Miss Ling Yin for their excellent work on the early stage of the design, to Prof. T. Katayama of University of Tokyo for his helpful suggestions, and to Dr. Chuan Zhang at IAP, Goethe-University, Frankfurt am Main, for the valuable discussions.

References

[1] J.W. Xia, W.L. Zhan, Y.J. Yuan, et al., Proceedings of APAC, THXMA03, 2007.
[2] Y.J. Yuan, H.W. Zhao, J.W. Xia, et al., Proceedings of CYCLOTRONS 2010, MOA2CIO01, 2010.
[3] Yuan He, Zhijun Wang, Chen Xiao, et al., Proceedings of IPAC 2011, WEPS052.
[4] J. Friedrich, A. Schempp, H. Deitinghoff, et al., Proceedings of EPAC92, 1992, p. 551.
[5] A. Schempp, Proceedings of PAC89', 1989, p. 1093.
[6] U. Ratzinger, K. Kaspar, E. Malwitz, et al., Proceedings of EPAC96', 1996, MOO07A.
[7] A. Schempp, Proceedings of LINAC96', 1996, p. 53.
[8] O .Kamigaito, A.Goto, Y.Miyazawa, Review of Scientific and Instruments 70 (1999) 4523.
[9] S. Koscielniak, L. Root, R. Lee, et al., Proceedings of LINAC96, 1996, p. 402.
[10] R. Duperrier, D. Uriot, N. Pichoff, et al., Proceedings of EPAC 2004 (2004) 2023.
[11] K.R. Crandall, T.P. Wangler, L.M. Young, et al., LA-UR-96-1836,2005.
[12] K.R. Crandall, R.H. Stokes, T.P. Wangler, Proceedings of the 1979 Linac Conference, 1979, BNL 51134, pp. 205–214.
[13] P. Lapostolle, M. Weiss, CERN-PS-2000-001 (DR), 2000.
[14] X.Q. Yan, R.A. Jameson, Y.R. Lu, et al., Nuclear Instruments and Methods in Physics Research A, 577 (2007) 402.
[15] X.Q. Yan, J.X. Fang, Z.Y. Guo, et al., Nuclear Instruments and Methods in Physics Research A, 554 (2005) 132.
[16] M. Reiser, Theory and Design of Charged Particle Beams, second ed., Wiley, New York, 2008.
[17] C. Zhang, Z.Y. Guo, A. Schempp, et al., Physical Review Special Topics—Accelerators and Beams 7 (2004) 100101.
[18] M. Comunian, A. Pisent, E. Fagotti, Proceedings of LINAC08, 2008, p. 145.
[19] Steven W. Williams, James M. Potter, IEEE Transactions on Nuclear Science, NS- 28 (1981) 2967.
[20] H. Klein, IEEE Transactions on Nuclear Science, NS- 30 (1983) 3313.